

**Donor states in modulation-doped Si/SiGe heterostructures**A. Blom,<sup>1</sup> M. A. Odnoblyudov,<sup>1,2</sup> I. N. Yassievich,<sup>1,2</sup> and K.-A. Chao<sup>1</sup><sup>1</sup>*Division of Solid State Theory, Department of Physics, Lund University, S-223 62 Lund, Sweden*<sup>2</sup>*A. F. Ioffe Physico-Technical Institute, Russian Academy of Science, 194021 St. Petersburg, Russia*

(Received 25 October 2002; revised manuscript received 7 February 2003; published 24 October 2003)

We present a unified approach for calculating the properties of shallow donors inside or outside heterostructure quantum wells. The method allows us to obtain not only the binding energies of all localized states of any symmetry, but also the energy width of the resonant states which may appear when a localized state becomes degenerate with the continuous quantum well subbands. The approach is nonvariational, and we are therefore also able to evaluate the wave functions. This is used to calculate the optical absorption spectrum, which is strongly nonisotropic due to the selection rules. The results obtained from calculations for Si/Si<sub>1-x</sub>Ge<sub>x</sub> quantum wells allow us to present the general behavior of the impurity states, as the donor position is varied from the center of the well to deep inside the barrier. The influence on the donor ground state from both the central-cell effect and the strain arising from the lattice mismatch is carefully considered.

DOI: 10.1103/PhysRevB.68.165338

PACS number(s): 73.20.Hb, 73.21.Fg, 78.67.De

**I. INTRODUCTION**

Impurity states in heterostructures have been the subject of detailed investigations during the last two decades. Traditionally, impurities are considered to be purely detrimental, by increasing the scattering rates. On the other hand, doping is essential to supply enough free carriers into the system. The strive has therefore been to remove the doping region from the active region by using modulation doping.

Recently, however, impurities have been placed in the active region of Si/SiGe quantum well structures to exploit their presence and properties for novel optical devices in the far-infrared or terahertz (THz) region.<sup>1-3</sup> Si and Ge are nonpolar materials with low intrinsic absorption at THz frequencies. Taking into account also the possibilities for integration with existing device technology,<sup>4</sup> these systems appear very attractive for optical applications in the THz region, which recently has received a lot of attention in a variety of fields.<sup>5</sup> A detailed knowledge of the properties of impurity states in Si/SiGe heterostructures is therefore essential.

Much effort has been spent on calculating the impurity energy states in a quantum well (QW). The techniques, all within the effective-mass approximation, range from the commonly employed variational techniques<sup>6-13</sup> to direct integration of the Schrödinger equation<sup>14</sup> and basis expansions.<sup>15,16</sup> The systems considered have, to the best of our knowledge, exclusively been III-V materials such as GaAs/Al<sub>x</sub>Ga<sub>1-x</sub>As quantum wells, for both donors<sup>6-11,14</sup> and acceptors,<sup>12,13,15,16</sup> and the results are found to agree reasonably well with experimentally obtained values.<sup>17-21</sup> Particular aspects such as image charges<sup>9</sup> and the effect of screening of the impurity potential by the free carriers in the well<sup>22</sup> have also been investigated.

To allow for a more detailed comparison of the calculated ground-state binding energy with experimental results, one must also take into account the central-cell effect or the chemical shift. Its physical origin is the absence of screening by the valence electrons at distances smaller than the outer electronic shells, in which case effective-mass theory breaks down. In principle, therefore, a proper treatment of chemical

shifts is not possible within the traditional effective-mass theory.<sup>23</sup> Nevertheless, several authors have considered the central-cell effect in the bulk by introducing various short-range pseudopotentials, which are adjusted to give agreement with the experimental binding energies.<sup>24-26</sup> This approach has also been attempted in the quantum well case,<sup>12</sup> whereas Mueller *et al.* have chosen to relate the QW central-cell shift to the envelope function amplitude.<sup>27</sup>

The donor ground state naturally appears below the lowest QW quantization level. As we will see, there are however Rydberg-like series of impurity states attached to each QW subband, as well as to the three-dimensional continuum. The situation is thus very similar to what has been observed in strong magnetic fields, where impurity states are attached to each Landau level.<sup>28</sup>

It has been noted by several authors that in narrow quantum wells, the lowest antisymmetric impurity state, which is bound to the second QW subband, may become resonant with the continuum of the first subband.<sup>8,9</sup> Resonant states of this so-called Fano type, i.e., a discrete (and hence localized) state degenerate with a continuum, are well known from atomic physics,<sup>29</sup> bulk semiconductors,<sup>24,30-33</sup> and quantum wells.<sup>34-37</sup> If symmetry allows it, the localized state can couple or hybridize with the continuous states. The resonant state is then characterized by an energy width, which is immediately related to its lifetime.<sup>29</sup> It is of crucial importance to determine this width in order to consider the effects of the coupled impurity states on the optical and electrical properties of modulation-doped quantum wells.

When the impurity is placed outside the well, in the barrier, similar but entirely different resonant states may also be formed from the usual shallow donor levels, and their widths can be evaluated by the resonant coupling method.<sup>38</sup> Attempts have been made to apply an essentially equivalent method for the case of donors inside the well.<sup>11,39,40</sup> It has however been shown that the approximations made in this approach are rather severe, and the widths do not agree with more exact results obtained using the same method as will be presented in this paper.<sup>41</sup> Only when the coupling between the impurity state and the quantum well is weak, can such

perturbation methods be expected to yield accurate results.

In this work we shall present a nonvariational approach for calculating the energy levels of shallow donors, in which we expand the total Hamiltonian in a complete basis. This turns the Schrödinger equation into a matrix eigenvalue problem, which is diagonalized to yield all localized, hybridized, and continuous states. The approach has several benefits over the variational method. First of all, no assumptions are made regarding the form of the impurity wave functions, but instead we obtain the correct envelope function, which then can be employed for calculating, e.g., optical matrix elements. Second, the entire energy spectrum is treated simultaneously, and hence we also obtain a description of the perturbed continuum and can observe the formation of the hybridized resonant states, and calculate their energy widths. Additionally, the difference in the effective mass in the well and barriers is easily included, as well as an electric field, and we are able to consider (but not limited to) anisotropic materials such as Si and Ge. It is furthermore possible to place the impurities in the barrier instead of in the well, and we thus have a unified approach for treating impurities in modulation-doped heterostructures.

We will specifically consider Si/Si<sub>1-x</sub>Ge<sub>x</sub> quantum wells, which are strained due to the lattice-constant mismatch. In result, the sixfold degeneracy of the conduction-band bottom and the donor states is partially lifted. Moreover, the impurity ground state in bulk Si is known to be shifted and split by the central-cell effect.<sup>42,43</sup> We shall therefore also present an approach for simultaneously taking the strain and the central-cell effect into account.

One of the advantageous properties of a coupled resonant state is the possibility of populating it by electrically pumping the carriers, from the bottom of the subband, until they reach the resonance energy.<sup>33,44,45</sup> They may then be captured into the resonant state, and possibly make an optical transition to the ground state. If an inverted population could be arranged between the resonant state and the ground state, one could realize a laser based on this process. A particularly appealing point of such a device is that since the impurity states are attached to the QW levels, it is possible to control the intraimpurity transition energy by varying the QW parameters. Experimental evidence of optical transitions involving coupled resonant states in quantum wells exists from both Raman scattering<sup>46</sup> and absorption spectroscopy<sup>47</sup> measurements. We therefore also calculate the impurity absorption spectrum for arbitrary polarization.

The remainder of our paper is outlined as follows. In Sec. II we present the nonvariational method for solving the Schrödinger equation of a shallow donor in a QW. Once the matrix eigenvalue problem is solved, the characterization of the eigenstates becomes an important issue, and this is discussed in Sec. III. The influence of strain and the central-cell effect is considered in Sec. IV, and in Sec. V we calculate the quantum well optical-absorption spectrum in the presence of coupled resonant states. The numerical results of the calculations for Si/Si<sub>1-x</sub>Ge<sub>x</sub> quantum wells are presented and discussed in Sec. VI, followed by a summary in Sec. VII.

## II. THE BASIS EXPANSION METHOD

We shall consider the problem of a shallow donor, described by the impurity potential  $V_c(\mathbf{r})$ , in a quantum well. Possibly an electric field  $\mathcal{E}$  along the QW growth direction  $z$  is also present. This field may be externally applied or built-in due to charge redistribution in the structure. In the effective-mass approximation, the total Hamiltonian can be written as

$$\hat{H} = \hat{H}_{\text{QW}} + V_c(\mathbf{r}) + e\mathcal{E}z, \quad (1)$$

with the quantum well Hamiltonian<sup>48</sup>

$$\hat{H}_{\text{QW}} = -\frac{\hbar^2}{2} \left( \frac{\partial}{\partial z} \frac{1}{m_{\perp}(z)} \frac{\partial}{\partial z} + \frac{1}{m_{\parallel}(z)} \nabla_{2\text{D}}^2 \right) + V(z). \quad (2)$$

From a principal point of view, our method allows for the quantum well potential profile  $V(z)$  to vary arbitrarily with the position  $z$ . We will however, for simplicity, choose  $V(z)$  to be a constant band offset  $U$  outside the well (which has width  $a$ ) and zero inside it. The effect of strain due to the lattice mismatch between the well and barrier regions is assumed to be incorporated in the band offset, except for the splitting of the donor ground state. This will be considered in detail in Sec. IV, along with the central-cell potential which is not included in the effective-mass Hamiltonian (1).

We wish to apply our method to anisotropic materials such as SiGe alloys. We have therefore split the kinetic-energy operator into two terms, and let the effective mass depend on the direction, with  $m_{\perp}$  and  $m_{\parallel}$  denoting the respective masses perpendicular and parallel to the two-dimensional (2D) QW plane. Further, note that the parallel and perpendicular are both taken to depend on the coordinate  $z$ , due to the presence of the heteroboundaries. In result, the Schrödinger equation with the Hamiltonian  $\hat{H}_{\text{QW}}$  will not be separable.

The dependence of the parallel mass  $m_{\parallel}$  on  $z$  is usually ignored in heterostructure calculations, since the electrons involved in in-plane transport are strongly confined to the QW channel. In the present case, this simplification is not appropriate since—especially for narrow wells—a large portion of the impurity wave function may appear in the barriers, and the binding energy depends critically on the exponentially decaying part of the wave function. The discontinuity of the parallel mass can alternatively be taken into account by introducing an effective well depth, which depends on the in-plane momentum,<sup>49</sup> but this is not convenient for our purposes. By diagonalizing  $\hat{H}_{\text{QW}}$  within our basis expansion method (see below), we find that a difference in the parallel masses leads to nonparabolicity of the QW subbands, but does not mix the different QW levels. [This is not to be confused with the nonparabolicity that arises from coupling to the valence band; cf. the discussion after Eq. (6).]

The impurity potential is taken as the Coulomb potential

$$V_c(\boldsymbol{\rho}, z) = -\frac{e^2}{\epsilon(z) \sqrt{\rho^2 + (z - z_0)^2}}, \quad (3)$$

(in CGS units) as is appropriate for a shallow donor located at  $(0,0,z_0)$ . Here  $\boldsymbol{\rho}$  is the radial vector in the QW plane. It has been demonstrated that the discontinuity in the dielectric constant  $\epsilon$  is of importance in GaAs/Al<sub>x</sub>Ga<sub>1-x</sub>As systems.<sup>9</sup> To take this into account properly, one could introduce image charges, but to evaluate the matrix elements with the resulting effective impurity potential (cf. Eqs. (5) and (6) in Ref. 13) would lead to rather extensive calculations in our present approach. Since the difference in the dielectric constant is small between Si and Si/Si<sub>1-x</sub>Ge<sub>x</sub> for small  $x$ , we will assume that  $\epsilon$  is a constant, independent of  $z$ .

Our method for solving the Schrödinger equation  $\hat{H}\Psi(\mathbf{r})=E\Psi(\mathbf{r})$  with the total Hamiltonian (1) is based on expanding the total wave function  $\Psi(\mathbf{r})$  in a complete basis and diagonalizing the Hamiltonian in this basis. As the basis, it is natural to use the quantum well eigenstates

$$|q\mathbf{k}\rangle = \frac{e^{i\mathbf{k}\cdot\boldsymbol{\rho}}}{2\pi} \varphi_q(z), \quad \langle q'\mathbf{k}'|q\mathbf{k}\rangle = \delta(\mathbf{k}-\mathbf{k}') \delta_{q,q'} \quad (4)$$

normalized as indicated, where  $q$  enumerates the QW levels and  $\mathbf{k}$  is the wave vector for the in-plane motion. These states diagonalize

$$\hat{H}_0 = \left[ -\frac{\hbar^2}{2} \frac{\partial}{\partial z} \frac{1}{m_{\perp}(z)} \frac{\partial}{\partial z} + V(z) \right] - \frac{\hbar^2}{2m_{\parallel}^w} \nabla_{2D}^2, \quad (5)$$

where  $m_{\parallel}^w$  is the effective mass inside the quantum well for the direction parallel to the QW plane.

The Hamiltonian  $\hat{H}_0$  differs from  $\hat{H}_{\text{QW}}$  in that the parallel effective mass  $m_{\parallel}$  does not depend on the  $z$  coordinate. Hence, in contrast to the case with  $\hat{H}_{\text{QW}}$ , the Schrödinger equation with the Hamiltonian  $\hat{H}_0$  is separable. To be complete, the basis must include both bound and unbound states, and we therefore enclose the system in a box of width  $\mathcal{L}_z$  in the  $z$  direction. The box is chosen large enough that it has negligible influence on the results. Nevertheless, the basis is complete for any size of the box. The additional boundary condition that  $\varphi_q(z)$  should vanish outside the box has to be taken into account also for the bound states to make them properly orthogonal to the unbound states.

The wave functions  $\varphi_q(z)$  can be found by standard methods,<sup>49</sup> and the energy eigenvalues are given by

$$\hat{H}_0|q\mathbf{k}\rangle = E_{qk}|q\mathbf{k}\rangle, \quad E_{qk} = E_q + E_k, \quad (6)$$

where  $E_q$  are the energies of the QW levels. In the simplest case the QW subbands are parabolic and  $E_k = \hbar^2 k^2 / 2m_{\parallel}^w$ . In principle one can however introduce here the realistic band dispersion, although it is necessary that the energy function  $E_k$  depends only on the magnitude  $k$  of  $\mathbf{k}$ . We stress that the discontinuity in the parallel effective mass  $m_{\parallel}$  (see above) is a separate issue; any nonparabolicity in the dispersion of the basis states is due to coupling to the valence bands and/or higher conduction bands.

Expanding in the complete orthonormal set  $|q\mathbf{k}\rangle$ , the total wave function can now be written as

$$\Psi(\mathbf{r}) = \sum_q \int d\mathbf{k} C_q(\mathbf{k}) |q\mathbf{k}\rangle. \quad (7)$$

An important benefit of the chosen basis is that  $\Psi(\mathbf{r})$  fulfills the QW boundary conditions by construction.

The spherical symmetry of the Coulomb potential is broken by the presence of the quantum well, and instead the total system adopts a cylindrical symmetry around the QW growth axis  $z$ . The total angular momentum  $\hat{\mathbf{L}}^2$  is hence not conserved, but its projection  $\hat{L}_z$  on the growth axis is. The eigenfunctions of  $\hat{L}_z$  are  $e^{-im\theta}$  with  $m=0, \pm 1, \pm 2, \dots$ , and they form a complete set. The same holds in Fourier space, and hence we can write

$$C_q(\mathbf{k}) = C_q(k, \theta_k) = \sum_{m=-\infty}^{\infty} i^{-m} e^{-im\theta_k} C_{qm}(k). \quad (8)$$

By inserting this into the expansion Eq. (7) and performing the angular integral, the eigenstates of the Hamiltonian  $\hat{H}$  given by Eq. (1) can be expressed as

$$\psi_m(\rho, \phi, z) = e^{-im\phi} \sum_q \varphi_q(z) \int_0^{\infty} k dk C_{qm}(k) J_m(k\rho), \quad (9)$$

where  $J_m$  is the  $m$ th-order Bessel function.

In principle one can diagonalize the total Hamiltonian  $\hat{H}$  using this form of the wave function, but it leads to several integrals that cannot be evaluated analytically. Instead, we insert expansion (7), taking into account the angular separation according to Eq. (8), into the Schrödinger equation  $\hat{H}\Psi(\mathbf{r})=E\Psi(\mathbf{r})$ . As expected from the cylindrical symmetry, the subspaces belonging to different projections  $m$  are not coupled to each other. We can therefore solve the problem—i.e., determine the expansion coefficients  $C_{qm}(k)$ —separately in each subspace (for a fixed  $m$ ).

The basis expansion turns the Schrödinger equation into a Fredholm integral equation of the second kind. It is customary to symmetrize such equations by multiplying both sides by  $\sqrt{k}$  and define

$$D_{qm}(k) \equiv \sqrt{k} C_{qm}(k). \quad (10)$$

The integral equation then takes the final form

$$\begin{aligned} \sum_{q'} \int_0^{\infty} dk' h_{qq'}^m(k, k') D_{q'm}(k') \\ = (E - E_{qk}) D_{qm}(k) \\ - \sum_{q'} [\mathcal{M}_{qq'}(k) + \mathcal{E}_{qq'}] D_{q'm}(k), \end{aligned} \quad (11)$$

where the Hermitian kernel

$$\begin{aligned} h_{qq'}^m(k, k') = \frac{-e^2 \sqrt{kk'}}{2\pi\epsilon} \int_{-\infty}^{\infty} dz \varphi_q^*(z) \varphi_{q'}(z) \\ \times \int_0^{2\pi} d\theta \frac{e^{-im\theta} e^{-|z-z_0|\alpha_{kk'}(\theta)}}{\alpha_{kk'}(\theta)} \end{aligned} \quad (12)$$

was calculated using the 2D Fourier transform of the Coulomb potential.  $\theta$  is the angle between  $\mathbf{k}$  and  $\mathbf{k}'$ , and  $\alpha_{kk'}(\theta) = \sqrt{k^2 + k'^2 - 2kk' \cos \theta}$ . The quantity

$$\mathcal{M}_{qq'}(k) = \frac{\hbar^2 k^2}{2m_0 m_{||}^w} \int_{-\infty}^{\infty} dz \varphi_q^*(z) \varphi_{q'}(z) \left( \frac{m_{||}^w}{m_{||}(z)} - 1 \right) \quad (13)$$

takes care of the discontinuity of the parallel mass  $m_{||}(z)$ , and the electric field  $\mathcal{E}$  enters through

$$\mathcal{E}_{qq'} = e\mathcal{E} \int_{-\infty}^{\infty} dz \varphi_q^*(z) z \varphi_{q'}(z). \quad (14)$$

To solve the integral equation we discretize the  $k$  axis and approximate the integral over  $k$  by a discrete sum. This turns the integral equation (11) into a matrix eigenvalue problem  $\mathcal{H}_{qq'}^{kk'} \mathcal{D} = E \mathcal{D}$ , where  $\mathcal{D}$  is a column vector of the (renormalized; see below) coefficients  $D_{qm}(k)$ . In the simplest (but most convenient) case we choose an equal step size  $\Delta k$  for the discretization, and the matrix elements are then given by

$$\mathcal{H}_{qq'}^{kk'} = (E_{qk} \delta_{q,q'} + \mathcal{M}_{qq'}(k) + \mathcal{E}_{qq'}) \delta_{k,k'} + h_{qq'}^m(k, k') \Delta k. \quad (15)$$

Due to the long-range nature of the Coulomb potential, a singularity appears in the kernel Eq. (12) for scattering in the forward direction. We do not explicitly consider screening in this work; instead the divergence is handled by averaging over small scattering angles.<sup>15</sup> In the case  $k = k' = 0$  the entire kernel vanishes exactly, but for other values of  $k = k'$  we obtain

$$\begin{aligned} h_{qq'}^m(k, k) &\approx \frac{-e^2 \sqrt{kk}}{2\pi\epsilon} \int_{-\infty}^{\infty} dz \varphi_q^*(z) \varphi_{q'}(z) \\ &\times \int_{\Delta k/2k}^{2\pi - \Delta k/2k} d\theta \frac{e^{-im\theta} e^{-|z-z_0|\alpha_{kk}(\theta)}}{\alpha_{kk}(\theta)} \\ &+ \frac{-e^2}{\epsilon\sqrt{\pi}} \delta_{q,q'} \quad (k \neq 0). \end{aligned} \quad (16)$$

A word on the normalization of the wave functions is appropriate. The matrix eigenvalue problem is solved by standard numerical methods, which return the eigenvectors  $\mathcal{D}^{(i)}$  and eigenvalues  $E^{(i)}$  for each eigenstate  $i$ . Typically such eigenvectors are normalized by  $\sum_{qk} |D_{qm}^{(i)}(k)|^2 = 1$ . Using the real-space density function

$$\begin{aligned} P^{(i)}(\mathbf{r}) &\equiv \int d\mathbf{r}' [\psi_m^{(i)}(\mathbf{r}')]^* \delta(\mathbf{r} - \mathbf{r}') \psi_m^{(i)}(\mathbf{r}) \\ &= \int_0^\infty dk \sqrt{k} J_m(k\rho) \int_0^\infty dk' \sqrt{k'} J_m(k'\rho) \\ &\times \sum_{qq'} [D_{qm}^{(i)}(k)]^* D_{q'm}^{(i)}(k') \varphi_q^*(z) \varphi_{q'}(z), \end{aligned} \quad (17)$$

the normalization condition of the corresponding wave function  $\psi_m^{(i)}(\mathbf{r})$  becomes (after discretization  $\int dk \rightarrow \sum_k \Delta k$ ),

$$1 = \int P^{(i)}(\mathbf{r}) d\mathbf{r} = 2\pi\Delta k \sum_{qk} |D_{qm}^{(i)}(k)|^2. \quad (18)$$

Thus the wave function  $\psi_m^{(i)}$  will be properly normalized if the physical coefficients  $D_{qm}^{(i)}(k)$  are taken as

$$D_{qm}^{(i)}(k) = \frac{\mathcal{D}_{qm}^{(i)}(k)}{\sqrt{2\pi\Delta k}}. \quad (19)$$

For the particular basis and QW potential profile we have chosen, most integrals that appear in the expressions above can be evaluated analytically, also when an electric field is included, leaving only a numerical integral over the angle  $\theta$ . The expressions are however much too lengthy to include here.

### III. CHARACTERIZATION OF THE EIGENSTATES

The diagonalization of the matrix problem provides the energies of all eigenstates of the Hamiltonian (1), and using Eq. (9) the corresponding eigenvectors allow us to evaluate the wave functions and hence matrix elements such as optical dipole-interaction strengths. It is however not immediately obvious how to identify the individual eigenstates as localized impurity states, QW band states, or hybridized states, and we shall now address this question.

We will adopt the notation of Ref. 9 and denote the case  $m=0$  by  $\Sigma$  and all other values by  $\Pi$ . If the impurity is placed in the center of the well, and there is no electric field present, the system is invariant under reflections  $z \rightarrow -z$ , and each eigenstate will also possess a quantum label  $g$  and  $u$  for even and odd parity, respectively. If this symmetry is broken, the only good quantum labels will be  $m$  and the energy  $E$ . It is however almost always possible to trace the eigenstates back to the symmetric situation, and we will therefore use eigenstate labels such as  $\Sigma_g$  even when asymmetry is present.

Our interest is particularly focused on the lowest antisymmetric impurity state, and we distinguish it from the other states of the same symmetry by referring to it as the  $\Sigma_u^*$  state. This state has been shown to be attached to the second QW subband, and for narrow well widths it becomes resonant with the continuum of the first (lowest) subband.<sup>8,9</sup> It was further demonstrated that the  $m = \pm 1$  or  $\Pi_u$  states do not become resonant, but instead remain attached to the lowest subband. We will therefore from now on specialize to the case  $m=0$  and often omit the label  $m$ .

In the absence of an electric field, we can always identify the states corresponding to the original QW levels (the subband bottoms) from the fact that these are the only eigenstates with nonzero contribution from the  $k=0$  basis states. To facilitate the further classification, we define for each eigenstate  $i$ , with energy  $E_i$ , a quantity

$$d_q(E_i) = 2\pi \int_0^\infty dk |D_q^{(i)}(k)|^2, \quad (20)$$

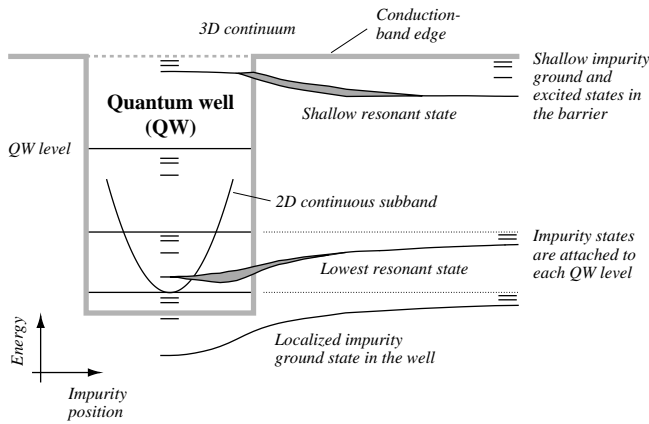


FIG. 1. Schematic picture, presenting the general behavior of how the various impurity states evolve as we change the impurity position, for a donor placed inside or outside a heterostructure quantum well. The shaded areas represent the energy width of the resonant states.

which measures the relative contribution to that eigenstate from the  $q$ th basis state  $\varphi_q(z)$ ; hence  $\sum_q d_q = 1$  for all states. The lowest QW level is taken as  $q=0$ .

Studying the values of  $d_q(E_i)$  for a particular eigenstate  $i$  now allows us to distinguish between three types of states.

(1) *Localized impurity states* only have contributions from higher QW levels, i.e., nonzero  $d_q$  only for levels  $q$  with energy  $E_q > E_i$ .

(2) *Continuous QW subband states* only have contributions from lower levels,  $E_q < E_i$ . (This is valid also in the case of a discontinuous parallel effective mass.)

(3) *Hybridized (coupled) resonant states* have contributions from both higher and lower levels.

Our method allows us to place the impurity anywhere in the system. Figure 1 summarizes the qualitative behavior of localized and resonant impurity states, as we change the impurity position from the middle of the quantum well to a remote location in the barrier. Some properties displayed schematically in this figure will be considered in more quantitative details in Sec. VI, whereas the remainder of this section will focus on the properties that characterize the various impurity states.

Any state appearing in the energy region below the lowest QW level must be localized. The lowest one will be the impurity ground state, which is split due to the central-cell effect (cf. Sec. IV). There are several  $\Sigma_g$  states attached to the lowest subband, and they form what resembles a Rydberg series, with decreasing binding energies converging towards the lowest subband edge. Actually, such series of localized states appear below each subband, i.e., each QW level has a set of impurity states attached to it (cf. Fig. 1). The binding energy of a localized state is therefore to be understood as the smallest energy required to place an initially localized electron into the corresponding QW subband. It is worth noting that these considerations also apply to the unbound QW levels. Hence if the well is so narrow that there exists no second bound QW level, all the  $\Sigma_u$  states are still well defined, but attached to the 3D continuum.

If the quantum well is wide enough, so that the binding

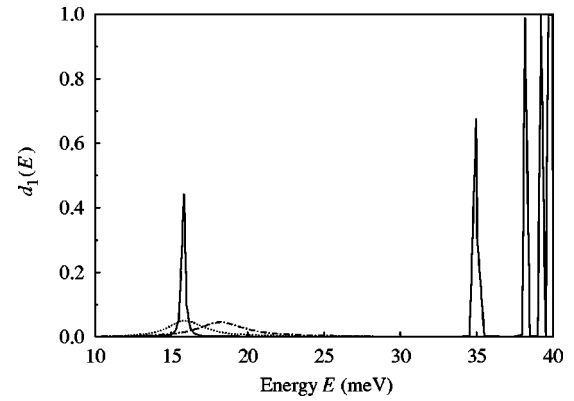


FIG. 2. The contribution  $d_1(E)$  of the second QW subband to the eigenstates in the energy range from the first QW level (at 10 meV) to the second one (at 40 meV). The width of the Si/Si<sub>0.9</sub>Ge<sub>0.1</sub> well is  $a=50$  Å, and the three curves correspond to different impurity positions  $z_0$ :  $z_0/a=0.05$  (solid), 0.25 (dotted), and 0.45 (dash-dot);  $z=0$  is the middle of the well. In addition to the resonances at 15–20 meV, similar ones resembling a Rydberg series appear close to the bottom of the second subband (for clarity this is only shown for  $z_0/a=0.05$ ).

energy of the lowest resonant state  $\Sigma_u^*$  is larger than the separation between the first ( $q=0$ ) and second ( $q=1$ ) QW levels, this state appears below the lowest QW level, and is therefore localized. It is, however, still attached to the  $q=1$  level. As the well width is decreased, the  $\Sigma_u^*$  state will therefore eventually appear in the continuum of the lowest QW subband, and we obtain a Fano resonant state—a localized state degenerate with a continuum. Similar resonant states can be formed from any excited impurity level (except those attached to the lowest subband) for suitable well parameters. We shall limit most of the discussion to the  $\Sigma_u^*$  state, but our approach can equally well be applied to any of the resonant states, of either parity.

As long as the impurity is placed in the center of the well, no hybridization or coupling can take place between impurity states that are resonant with subbands of opposite parity. The localized  $\Sigma_u^*$  state is attached to the  $q=1$  QW level, and therefore  $d_0(E_{\Sigma_u^*})=0$  in the symmetric situation. Moreover, without any hybridization,  $d_q = \delta_{q,0}$  for the continuous states belonging to the lowest QW level. Coupling will however be present as soon as any asymmetry that breaks the parity conservation is introduced—such as shifting the impurity position or applying an electric field. The localized state is then “diluted” throughout a band of actual stationary states, whose profile is represented by a Lorentzian resonance curve.<sup>29</sup> This hybridization mixes a certain amount of continuum into the  $\Sigma_u^*$  state (giving  $d_0(E_{\Sigma_u^*}) \neq 0$ ), and the continuous states acquire a partly localized character ( $d_1 \neq 0$ ). Thus the degree of hybridization is measured by the coefficients  $d_1(E_i)$ , and the resonance profile is exactly given by these coefficients when plotted against the eigenenergies  $E_i$  in the region between the first and second QW levels (cf. Fig. 2). If the electron is initially placed in the coupled resonant impurity state, it will autoionize with a mean lifetime  $\tau$

$=\hbar/\Gamma$  determined by the energy width  $\Gamma$  of the resonant state.<sup>29</sup> We can calculate this width by fitting a Lorentzian to the resonance profile.

In the barrier, the binding energies—which are still measured relative the corresponding QW levels—decrease towards zero, although not very rapidly. As the impurity is moved further away from the well, each impurity state remains bound to its initial QW level, with vanishing binding energy. Hence, even at very large impurity distances, the impurity “ground state” appears to be a deep state with an energy defined by the lowest QW level. This is counterintuitive; we expect the impurity ground state to be a shallow state bound to the 3D continuum. However, the electron density of the deep impurity states is actually localized close to the center of the well, and not on the impurity. When the distance to the well increases, their wave functions become more and more symmetric around the center of the well and assume the shape of the QW basis functions  $\varphi_q(z)$ . At the same time these wave functions are extended in the radial direction in the QW plane due to the smaller binding energy. This behavior can be understood from the fact that the electronic density is determined by the effective potential in the well, and when the impurity is far away, the tail of the Coulomb potential is much weaker than the QW confinement potential. At large impurity distances, the Coulomb potential and the well are almost (but not completely) decoupled, which means that the deep donor states essentially derive from a single QW level, which can be verified by studying the coefficients  $d_q$ . Similar observations have been made by Stopa and DasSarma<sup>14</sup> who also use a nonvariational technique to treat donors in GaAs quantum wells.

As was stated above, there are also QW impurity states attached to the 3D continuum (cf. the upper-right part of Fig. 1). When the impurity is in the barrier, these states are the familiar ground and excited shallow donor states, with the electron density localized at the impurity position. We can now study what happens to an initially decoupled shallow donor as it is moved closer to the quantum well. Due to the induced coupling, Rydberg-like series of impurity states—localized in the well—are pushed down from each continuum edge, i.e., from each QW level. The lowered symmetry due to the presence of the quantum well causes mixing between the hydrogenic  $n$  and  $\ell$  levels (actually only between levels for which  $\Delta\ell$  is an even number<sup>14</sup>), and only  $m$  remains as a good quantum label. The original shallow donor state broadens due to the coupling,<sup>38</sup> but remains bound to the 3D continuum also when the impurity finally is located in the well. If the electron is initially placed in the shallow donor state outside a quantum well, it will after some time tunnel into the QW. The tunneling time is essentially given by the energy width of the resonant shallow state, which can be calculated within our basis expansion approach or as in Ref. 38.

#### IV. STRAIN AND CENTRAL-CELL EFFECTS

In order to compare calculated results for the ground-state binding energy of donors in Si quantum wells with experimental values, it is essential to take into account the effects

of both strain and the central-cell shift. Although there would, in principle, be some central-cell splitting also of the excited states, this effect is expected to be very small.<sup>42</sup> This is especially true for the odd-parity states, since they have a vanishing envelope function at the impurity position. Thus the energy of the resonant  $\Sigma_u^*$  state, which in the bulk limit corresponds to the  $2p_0$  hydrogenic state, will not be affected, and we shall in this section only be concerned with the impurity ground state.

The conduction-band minimum in bulk Si lies at about  $\Delta_1 = (0,0,0.85)$  in units where the  $X$  point is  $(0,0,1)$ , with six equivalent valleys. Hence the donor  $1s$  ground state would be sixfold degenerate. Experimentally, however, one instead observes three levels, with binding energies  $E_b + \Delta_0$  (the nondegenerate true ground state),  $E_b + \Delta_0 - \Delta_E$  (twofold degenerate), and  $E_b + \Delta_0 - \Delta_T$  (threefold degenerate). Here  $E_b$  is the effective-mass binding energy, which according to Kohn and Luttinger<sup>42</sup> is about 29 meV in Si. The energies  $\Delta_0$ ,  $\Delta_E$ , and  $\Delta_T$  are positive and, in contrast to  $E_b$ , depend on the particular impurity species. This additional contribution to the binding energy is known as the central-cell effect or chemical shift, and is in general determined from comparisons with experimental values. In the case of P donors in Si,  $\Delta_0 \approx 16.6$  meV (or 14.3 meV if one uses the effective-mass value  $E_b = 31.27$  meV from the more elaborate calculations by Faulkner<sup>50</sup>),  $\Delta_E \approx 13.0$  meV and  $\Delta_T \approx 11.7$  meV.<sup>51</sup>

The chemical shift is usually considered as arising from a strong potential acting only very near the impurity center. Although, as discussed in the Introduction, a proper treatment is not strictly possible in effective-mass theory, one could try to incorporate the central-cell effect by employing a short-range pseudopotential. This, however, fails when applied to a basis expansion method, since this potential now interacts not with the total wave function (as is the case in a variational calculation) but with the individual basis states. If one adjusts the pseudopotential parameters to produce agreement with experimental binding energies for a certain well width (such as a very wide one, close to bulk), the parameters will not give any sensible results when the basis is different, say, for a narrow well. Instead, we will here show how to relate the QW central-cell shift to the bulk shifts, purely by symmetry considerations.

In the effective-mass approximation, the wave functions are written as  $\Phi(\mathbf{r}) = \phi(\mathbf{r})u(\mathbf{r})$ , where the envelope function  $\phi$  varies slowly over interatomic distances, and the Bloch function  $u$  is rapidly varying and describes the region close to the atomic nuclei. In Si there are six equivalent conduction-band minima or valleys  $\ell$ , which we index by  $\ell \in \{x, \bar{x}, y, \bar{y}, z, \bar{z}\}$  ( $\bar{x}$  is shorthand for  $-x$ ). Hence one must generally consider linear combinations  $u(\mathbf{r}) = \sum_{\ell} \alpha_{\ell} u_{\ell}(\mathbf{r})$  of the Bloch functions  $u_{\ell}$  of each valley bottom. If we denote the (unspecified) central-cell potential by  $V$ , the nonzero matrix elements between the valley bottom Bloch functions in Si are<sup>52</sup>

$$\langle u_{\ell} | V | u_{\ell'} \rangle = \begin{cases} V_0, & \ell = \ell' \\ V_g, & \ell = -\ell' \\ V_f, & |\ell| \neq |\ell'|. \end{cases} \quad (21)$$

By evaluating the matrix elements  $\langle \Phi_{1s}^i | V | \Phi_{1s}^j \rangle$  for the six  $1s$  donor states  $\Phi_{1s}^i(\mathbf{r})$ , we can relate the parameters  $V_0$ ,  $V_f$ , and  $V_g$  to the observed impurity binding energies as follows:

$$\begin{aligned} V_0 |\phi_{1s}(\mathbf{r}_0)|^2 &= (3\Delta_T + 2\Delta_E - 6\Delta_0)/6, \\ V_g |\phi_{1s}(\mathbf{r}_0)|^2 &= (2\Delta_E - 3\Delta_T)/6, \\ V_f |\phi_{1s}(\mathbf{r}_0)|^2 &= -\Delta_E/6, \end{aligned} \quad (22)$$

where  $\mathbf{r}_0$  is the impurity position and  $\phi_{1s}$  is the  $1s$  envelope function. For further details, see Appendix A.

We now consider donors placed in a Si quantum well, grown pseudomorphically between (unstrained)  $\text{Si}_{1-x}\text{Ge}_x$  barriers. This case differs compared to bulk Si in two ways. First, the Si region will be strained due to the lattice-constant mismatch between Si and Ge. Second, the envelope function is different due to the additional confinement. On the other hand, it is reasonable to assume that the matrix elements  $V_0$ ,  $V_g$ , and  $V_f$  are unchanged, since the central-cell potential  $V$  is appreciable only in a region much smaller than the well width. Hence, we can still use the values of these parameters, as obtained from Eq. (22) using the bulk binding energies (determined by  $\Delta_0$ ,  $\Delta_E$  and  $\Delta_T$ ), but replace  $\phi_{1s}$  by the QW envelope function.

By taking into account the effects of strain and the central-cell shifts simultaneously, one finds—in addition to an overall shift—that for (001)-grown wells, the sixfold degenerate donor ground state splits into five energy levels, whereof one is twofold degenerate.<sup>43</sup> The details of this calculation are presented in Appendix B. The lattice constant of unstrained  $\text{Si}_{1-x}\text{Ge}_x$  bulk alloy has been parametrized<sup>53</sup> from experimental data<sup>54</sup> as

$$a(x) = a(\text{Si}) + 0.020\,032\,6x(1-x) + [a(\text{Ge}) - a(\text{Si})]x^2,$$

where  $0 \leq x \leq 1$  and  $a(\text{Si})$  and  $a(\text{Ge})$  are the lattice constants of bulk Si and Ge (in nanometers). Inserting this into Eqs. (B4) and (B5) we find that the strain component parallel to the QW interfaces  $e_{||} > 0$  and hence the strain parameter  $\xi = -\Xi_u e_{||} (2C_{12}/C_{11} + 1)/3$  defined in Eq. (B10) is negative. Here  $\Xi_u$  is the deformation potential and  $C_{ij}$  are the components of the stiffness tensor. Even with only a small content  $x$  of Ge, the condition that the strain splitting is large compared to the central-cell shifts ( $\xi \gg \Delta_0$ ) is fulfilled.<sup>53</sup> Therefore, from the results in Appendix B, the lowest valleys will be  $\Delta_{\perp}$ , perpendicular to the QW interfaces, to which two donor states are attached. Four other donor states are associated with the higher  $\Delta_{||}$  valleys, which are strain split from  $\Delta_{\perp}$  by  $3|\xi|$ .

In our calculations we assume that the strain splitting of the conduction band is included in the band offset  $U$ , and consider only the two lowest donor states belonging to  $\Delta_{\perp}$ . These two states are shifted from the QW effective-mass value  $E_b$  by

$$\frac{|\psi_{\text{QW}}(\mathbf{r}_0)|^2}{|\phi_{1s}(\mathbf{r}_0)|^2} \left[ -\Delta_0 + \begin{cases} 2\Delta_E/3 \\ \Delta_T \end{cases} \right]. \quad (23)$$

The Bloch functions of the two states are the symmetric and antisymmetric combinations of the two  $\Delta_{\perp}$  valleys. The quantum well envelope function amplitude  $|\psi_{\text{QW}}(\mathbf{r}_0)|^2$  is obtained from the basis expansion coefficients using Eq. (17). We will return to the question how to correctly determine the bulk amplitude  $|\phi_{1s}(\mathbf{r})|^2$  in Sec. VI.

The central-cell shifts are negative, which means that the binding energies are increased. The impurity ground state now corresponds to the (nondegenerate)  $2\Delta_E/3$  state, since  $\Delta_E \approx \Delta_T$  for typical donors (P, As, Sb) in Si.<sup>51</sup> It is worth noting that, since furthermore  $\Delta_E \approx \Delta_0$ , the central-cell effect in the quantum well case can be much smaller than in bulk Si, at least if the ratio of the wave functions is not too large. In bulk Si, the donor ground state is shifted by  $\Delta_0 = 17$  meV, but in the QW the ground state shift for P donors is only  $\Delta_0 - 2\Delta_E/3 \approx 8$  meV, assuming that the envelope function ratio in Eq. (23) is of the order unity. On the other hand, this ratio is expected to be above unity for narrow wells, due to the additional confinement, and so in this case the central-cell effect further increases the already enhanced ground-state binding energy.

## V. OPTICAL ABSORPTION

If the impurity is placed exactly in the middle of the well (and no electric field is present), the selection rules prohibit the radiative decay from the lowest subband to the impurity ground state by a dipole transition with polarization parallel to the QW growth direction. However, if some asymmetry is introduced, the transition is allowed from the part of the subband which is hybridized with the resonant antisymmetric  $\Sigma_u^*$  impurity state.

In the dipole approximation, Fermi's golden rule gives the probability per unit time of optical absorption, at the frequency  $\omega$ , between states  $i$  (initial) and  $j$  (final) as

$$W_{ji} = \frac{2\pi}{\hbar} \left( \frac{eA_0}{mc} \right)^2 |\langle j | \hat{\mathbf{e}} \cdot \hat{\mathbf{p}} | i \rangle|^2 \delta(E_j - E_i - \hbar\omega), \quad (24)$$

where  $A_0$  is the magnitude of the electromagnetic vector potential,  $\hat{\mathbf{e}}$  is the photon polarization vector,  $\hat{\mathbf{p}}$  is the momentum operator, and  $E_i$  is the energy of eigenstate  $i$ .

Assuming that the system contains  $N$  independent impurities, we may relate the absorption rate  $W_{ji}$  to the absorption coefficient  $\mathcal{A}$  as

$$\mathcal{A}(\hbar\omega) = \frac{N}{\Omega} \frac{2\pi\hbar c}{\kappa\omega|A_0|^2} \sum_j W_{ji}, \quad (25)$$

where  $\Omega$  is the total sample volume and  $\kappa$  is the refraction index. In a quantum well, a more natural quantity to consider is the absorption cross section

$$\sigma = \frac{\mathcal{A}\Omega}{N} = \frac{4\pi^2\hbar^2\alpha}{\kappa} \sum_j \left| \left\langle j \left| \frac{\hat{\mathbf{e}} \cdot \hat{\mathbf{p}}}{m} \right| i \right\rangle \right|^2 \frac{\delta(\hbar\omega_{ji} - \hbar\omega)}{\hbar\omega_{ji}}, \quad (26)$$

where  $\omega_{ji} = (E_j - E_i)/\hbar$  and  $\alpha \equiv e^2/\hbar c$  is the fine-structure constant.

The summation in Eq. (26) in principle involves, among other things, final states  $j$  in all valleys with any spin polarization. We can however ignore the four  $\Delta_{\parallel}$  valleys altogether, since the strain splitting is much larger than the impurity binding energy. We shall consider absorption only from the ground state, and so the initial state  $i$  is an equal mix of the two  $\Delta_{\perp}$  valleys, as discussed in Sec. IV, with fixed (but arbitrary) spin. The dipole operator  $\hat{\mathbf{e}} \cdot \hat{\mathbf{p}}$  does not affect spin and connects only the parts of the initial and final states belonging to the same valley. This holds also when the temperature is large enough that the occupation probabilities of the two states  $u_2$  and  $u_6$  (cf. Appendix B) are roughly equal; in this case we must also average over the two states. Thus the sum over  $j$  can be restricted to a sum over the final energy  $E$  and the different cylindrical subspaces. It is furthermore enough to evaluate the matrix element between the envelope functions only, as long as we replace the electron mass  $m$  by the effective mass  $m^*$  in the direction parallel to  $\hat{\mathbf{p}}$ .<sup>49</sup>

Since one would most naturally place the donors inside the QW for optical applications of this kind, we assume that the relevant effective masses are those of the well, and write

$$\frac{\hat{\mathbf{e}} \cdot \hat{\mathbf{p}}}{m^*} = \frac{\cos \theta \hat{p}_x}{m_{\parallel}^w} + \frac{\sin \theta \hat{p}_z}{m_{\perp}^w}, \quad (27)$$

where  $\theta$  is the angle between the photon  $\mathbf{k}$  vector and the QW growth direction  $z$ . The light is assumed to be plane polarized in the plane spanned by the normal to the QW plane and the photon  $\mathbf{k}$  vector. The  $x$  axis is defined as the intersection of this plane and the QW interface planes.

In principle Eq. (27) allows for interference between the two terms when inserted into Eq. (26). The interference terms are essentially  $\langle i | \hat{p}_x | j \rangle \langle j | \hat{p}_z | i \rangle$  or the complex conjugate thereof, to be summed over all final states  $j$ . Here  $i$  is the impurity ground state, which belongs to the  $m_i = 0$  cylindrical subspace. The sum over final states can be split into two parts, where we first consider all states  $j$  in a particular subspace  $m_j$ , and then sum over all subspaces. The first factor is  $\langle i | \hat{p}_x | j \rangle \propto \delta_{m_j, m_i \pm 1}$ , which follows from the selection rule  $\Delta m = \pm 1$  (see below) for the  $\hat{p}_x$  operator. On the other hand,  $\langle j | \hat{p}_z | i \rangle \propto \delta_{m_j, m_i}$  since  $\Delta m = 0$  for  $\hat{p}_z$ . Thus, the interference terms vanish, and we may write

$$\sigma = \sigma_x \cos^2 \theta + \sigma_z \sin^2 \theta, \quad (28)$$

which defines  $\sigma_x$  and  $\sigma_z$ . As we will see in Sec. VI, the absence of interference is a contributing factor to producing a symmetric absorption peak.

Let us first consider  $z$  polarization. To eliminate the  $\delta$  symbol in Eq. (26) we turn the sum over final states  $j$  into an integral. However, we have to consider that the relevant density of final states in this case is not the usual 2D density of states. If we double the ‘‘size’’ of our system ( $\Delta k \rightarrow \Delta k/2$ ) we only get twice as many eigenstates, since the discretization in Sec. II is carried out over the magnitude  $k$  of  $\mathbf{k}$ . Hence the density of states in  $k$  space is  $dn/dk = 1/\Delta k$ , and in energy space

$$\frac{dn}{dE_k} = \frac{dn}{dk} \frac{dk}{dE_k} = \frac{1}{\hbar \Delta k} \sqrt{\frac{m_{\parallel}^w}{2E_k}}, \quad (29)$$

where the parabolic dispersion relation  $E_k = \hbar^2 k^2 / 2m_{\parallel}^w$  was again assumed. The presence of  $\Delta k$  will properly renormalize the matrix element when this is evaluated from the discretized expansion coefficients (cf. the discussion on normalization in Sec. II). Now we may perform the integral over energy to remove the  $\delta$  function, and the absorption cross section can be evaluated at  $\omega = \omega_{ji}$  for all eigenstates  $j$ . The result is

$$\sigma_z = \frac{2\pi^2 \alpha}{\kappa \Delta k} \frac{\sqrt{2\hbar m_{\parallel}^w}}{\hbar (m_{\perp}^w)^2 \omega_{ji}^{3/2}} |\langle j | \hat{p}_z | i \rangle|^2. \quad (30)$$

By using the form Eq. (9) of the wave function for the states  $i$  and  $j$  (belonging to the subspaces  $m$  and  $m'$ , respectively), the remaining matrix element becomes

$$\begin{aligned} \langle j | \hat{p}_z | i \rangle &= \int_0^{2\pi} d\phi e^{-i(m-m')\phi} \sum_{qq'} \langle q' | \hat{p}_z | q \rangle \int_0^{\infty} dk D_{qm}^{(i)}(k) \\ &\quad \times [D_{q'm'}^{(j)}(k)]^*. \end{aligned} \quad (31)$$

Since the first integral yields  $2\pi \delta_{m,m'}$ , we obtain the selection rule  $\Delta m = 0$  for this polarization. The integral over  $k$  can be evaluated from the matrix eigenvectors  $\mathcal{D}$ , taking the normalization relation Eq. (19) into account. We can furthermore use the commutator  $[\hat{H}_{\text{QW}}, z] = -i\hbar \hat{p}_z / m_{\perp}(z)$  and the fact that the states  $q$  and  $q'$  are eigenstates of  $\hat{H}_{\text{QW}}$ , defined in Eq. (2), to rewrite

$$\langle q' | \hat{p}_z | q \rangle = \frac{i}{\hbar} (E_{q'} - E_q) \int_{-\infty}^{\infty} \varphi_{q'}^*(z) z m_{\perp}(z) \varphi_q(z) dz. \quad (32)$$

Next we consider  $x$  polarization, for which the selection rule is  $\Delta m = \pm 1$ , as will be demonstrated shortly. We will focus on the energy region between the first and second QW subbands, where the lowest resonant state  $\Sigma_u^*$  appears. Since there are no resonant states with  $m = \pm 1$  in this region, and since the ground state belongs to the  $m = 0$  subspace, we can ignore mixing of the QW subbands and represent the final states as normalized plane waves belonging to the first subband  $q = 0$ :

$$|j\rangle = \frac{\exp(i\mathbf{k}^{(j)} \cdot \boldsymbol{\rho})}{\mathcal{L}} \varphi_{q=0}(z), \quad (33)$$

where  $\mathcal{L}$  is the normalization length.

To derive the selection rule, one may rewrite the momentum operator  $\hat{p}_x$  in cylindrical coordinates and act on the cylindrical expansion of a plane wave  $e^{i\mathbf{k} \cdot \boldsymbol{\rho}} = \sum_m i^m e^{-im\vartheta} J_m(k\rho)$ , where  $\vartheta$  is the angle between the vectors  $\mathbf{k}$  and  $\boldsymbol{\rho}$ . One then obtains

$$\langle j | \hat{p}_x | i \rangle = \frac{\pi \hbar k_x^{(j)}}{\mathcal{L}} C_{q=0}^{(i)}(k^{(j)}) \sum_{m=-\infty}^{\infty} \delta_{m, \pm 1} \quad (34)$$

which shows the selection rule explicitly; the summation is trivial and gives a factor of 2. As before,  $i$  refers to the donor ground state, represented by an expansion of form (9). It is not surprising that the momentum operator  $\hat{p}_x$  picks up the  $x$  component of the final wave vector  $\mathbf{k}^{(j)}$ ; the result Eq. (34) can of course also be obtained by acting with  $\hat{p}_x$  on the plane wave  $e^{i\mathbf{k}\cdot\boldsymbol{\rho}}$  without changing to cylindrical coordinates. But in that case the selection rule will not appear, since it is not actually present in the final result, after the summation in Eq. (34) has been carried out.

We remove the  $\delta$  function in Eq. (26) by integrating with the usual 2D density of states per spin  $\mathcal{L}^2 m_{\parallel}^w / 2\pi\hbar^2$ . In result, we arrive at

$$\sigma_x = \frac{2\pi^2\alpha}{\kappa\Delta k} \frac{\hbar K_{q=0,j}}{m_{\parallel}^w \omega_{ji}} |\mathcal{D}_{q=0}^{(i)}(K_{q=0,j})|^2, \quad (35)$$

where  $K_{qj}$  is defined from the energy conservation relation

$$E_i + \hbar\omega_{ji} = E_q + \frac{\hbar^2 K_{qj}^2}{2m_{\parallel}^w}, \quad (36)$$

where  $E_i$  is the energy of the donor ground state and  $E_q$  is the energy of the  $q$ th QW level. The expansion coefficient  $\mathcal{D}_q^{(i)}(K_{qj})$  can be found by interpolating the matrix eigenvectors over  $k$ .

## VI. RESULTS

### A. Numerical aspects

In this section we present numerical results for shallow Coulombic donors in (001)-grown Si/Si<sub>1-x</sub>Ge<sub>x</sub> quantum wells. The electronic parameters (effective masses, band offsets, and deformation potentials) of these systems are known from the systematic study by Rieger and Vogl.<sup>53</sup> We make the approximation, as discussed in Sec. II, that the difference in the dielectric constant can be ignored, and use that of bulk Si throughout. Furthermore, although the nonparabolicity of the subbands in strained Si quantum wells has been found to be considerable, we take the basis subbands to be parabolic, since the nonparabolicity parameter is not well known.<sup>55</sup> For small contents  $x$  of Ge the effective masses are very similar for the well and barrier regions, and therefore the discontinuity in the parallel effective mass turns out to have no observable influence on the results for these particular systems.

For the matrix problem to be of finite order we must limit the number of QW levels to include in the basis, and also the integration (sum) over  $k$  must be cut off somewhere. This is the only real approximation in the method (other than those inherent in effective-mass theory). Therefore, in order to assure the numerical accuracy of our results, we always include all bound QW levels, and increase the number of unbound levels until the eigenvalues do not change. The same procedure is applied to determine the required density and range of  $k$  values. The contribution from the unbound states drops off rapidly with increasing energy, although for narrower wells it is naturally important to include more unbound states.

With a sparser basis set it naturally becomes impossible to resolve all the (infinitely many) excited impurity states close to the bottom of each subband. These states are however usually well separated from the lowest resonant states that we are mainly interested in. Nevertheless, if the situation occurs when there are several impurity levels in very close vicinity of each other, e.g., if the binding energy of the ground state is very small, the basis must naturally be chosen denser, so that all states of interest are resolved. Furthermore, the density of  $k$  points must always be large enough that the resonance width is covered by more than just a few points. In the results presented below, these issues have been carefully taken into account.

Quite a large range of  $k$  values is needed to reach convergence, especially in the ground-state wave-function amplitude, since the expansion coefficients decay rather slowly, roughly as  $k^{-3.5}$ . This means that, since at the same time one wishes to keep  $\Delta k$  as small as possible for accuracy, the  $N \times N$  matrix problem becomes fairly huge (typically  $N$  will be between 1000 and 2000). The size of the matrix problem which can be diagonalized is a limiting factor, and it is not always possible to obtain optimal accuracy, especially for very wide wells. Nevertheless, we have made sure that the errors in the results presented here are less than 1%. The only exceptions are the energy width of the resonant state when the impurity is deep inside the barrier (in which case the width itself is very small) and the ground-state wave-function amplitude; here the errors may be up to 5%. However, the accuracy in the *ratio* of the wave-function amplitude to the corresponding bulk value—which really is the quantity of interest—is much better than the accuracy of the amplitude itself. The wave-function amplitudes are also more sensitive to the size of the outer box  $\mathcal{L}_z$  (which normalizes the “continuum” basis functions) than the eigenvalues are. Again, the convergence can be controlled by increasing this size as much as needed.

### B. Binding energy and resonant-state energy width

In agreement with variational calculations, we find that the binding energies are generally increased due to the additional confinement presented by the quantum well potential, both for the ground and the excited states (cf. Figs. 3 and 4). Furthermore, since the  $\Sigma_u^*$  state is attached to the second QW level, it appears at higher and higher energies as the level separation increases with smaller well widths. This holds until the well becomes very narrow, when the binding energies decrease again, as shown in Fig. 3. When the well width is much smaller than the radius of the impurity state, one can view the system as an impurity situated in the 3D bulk, slightly perturbed by the narrow quantum well. For a vanishingly narrow well the binding energies therefore approach the values corresponding to the bulk barrier material. Moreover, below a certain well width there is no bound odd-parity QW level, and the  $\Sigma_u^*$  state then becomes attached to the continuum, which does not move as the well width is changed. These effects on the ground- and resonant-state binding energies have also been observed in variational calculations.<sup>9,14</sup>

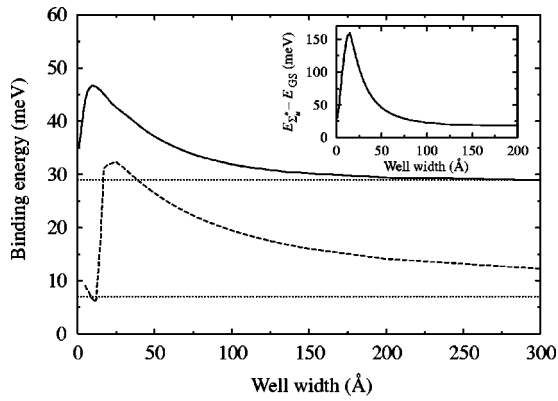


FIG. 3. The binding energy of the ground state (solid curve) and the  $\Sigma_u^*$  state (dashed curve) for a Si/Si<sub>0.8</sub>Ge<sub>0.2</sub> quantum well of varying width. The impurity is located in the middle of the well, and the central-cell shift is not included. For wide wells the binding energies approach the bulk values (29 meV and 7 meV, respectively), indicated by the dotted lines. The inset shows the energy separation between the  $\Sigma_u^*$  state and the ground state (GS).

For wide wells, the ground-state binding energy converges to the effective-mass value of the bulk hydrogenic 1s donor state in Si at a width of about 250 Å, which is faster than for GaAs/Al<sub>x</sub>Ga<sub>1-x</sub>As quantum wells.<sup>9</sup> Clearly, the reason is the smaller radius of the impurity states in Si compared to GaAs. By the same reasoning, the convergence of the excited  $\Sigma_u^*$  state to the corresponding bulk state 2p<sub>0</sub> is slower than for the ground state, since the smaller binding energy of the excited state corresponds to a larger radius of the state. From Fig. 4 we further note that for uniformly doped wells, one effectively obtains broad bands of impurity energies, instead of a set of sharp levels. The bandwidth of the ground state can be almost comparable to the spacing of

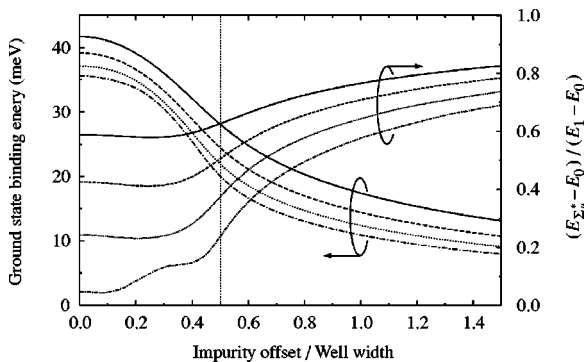


FIG. 4. The impurity ground-state binding energy (left-hand vertical axis) for Si/Si<sub>0.8</sub>Ge<sub>0.2</sub> wells of widths (from top to bottom)  $a=30$  Å, 40 Å, 50 Å, and 60 Å, and for the same widths and symbols the position of the resonant  $\Sigma_u^*$  state (right-hand vertical axis). The right-hand vertical scale is normalized so that 0 corresponds to the first QW level, and 1 to the second one. The QW level energies are, from the narrowest (30 Å) to the widest (60 Å) well:  $E_0=26.8, 17.1, 11.8, 8.7$  meV and  $E_1=102.7, 67.1, 46.8, 34.4$  meV. The vertical line marks the edge of the well, and the impurity offset is measured from the middle of the well. The central-cell shift is not included.

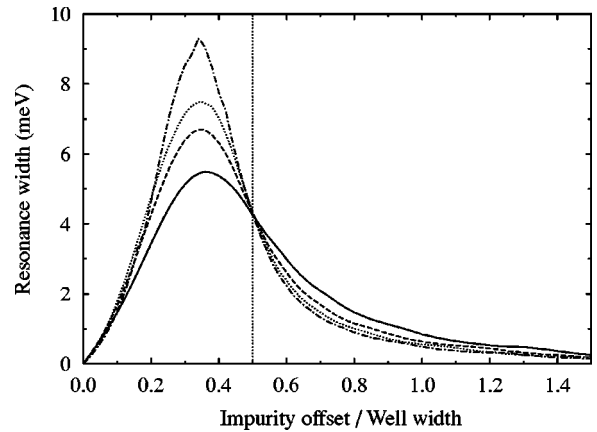


FIG. 5. The energy width  $\Gamma$  of the resonant  $\Sigma_u^*$  state for the same quantum wells as in Fig. 4, with the same symbols for the curves.

the QW levels, in particular if the central-cell effect is also taken into account (see below).

The decay of the binding energies in the barrier is very slow. It follows a power-law dependence, but there does not appear to exist any common exponent; for the curves shown in Fig. 4 the exponents are  $\approx 0.7-0.8$  for the ground state and  $0.2-0.4$  for the resonant state. Nevertheless, at very large distances the impurity states coalesce with the quantum well levels; see the discussion in Sec. III regarding the impurity wave functions when the donor is placed in the barrier.

Figure 5 shows the energy width  $\Gamma$  of the resonant  $\Sigma_u^*$  state. As the impurity is moved away from the center of the well, the width increases due to the enhanced coupling (the increased asymmetry); this could also be seen from Fig. 2. When we continue to move towards the barrier,  $\Gamma$  reaches a maximum value at about 35% offset. After that, it decreases due to the reduced overlap between the two lowest QW basis functions. In the barrier, the width continues to decay according to a power-law dependence with an exponent (which is not common for different well widths) of the order 2–3. This is in contrast to the resonant state formed from the shallow donor states when the impurity is in the barrier (shown in the upper-right part of Fig. 1), for which the width decays exponentially.<sup>38</sup>

For the same relative impurity offset, the resonance is broader in wider wells, which is an effect of the fact that the  $\Sigma_u^*$  state appears closer to the bottom of the band. In Fig. 2 the same can be observed for the higher excited  $\Sigma_u$  resonant states, which are narrower the higher energy they have. We furthermore see from Fig. 2 that a widening of the resonance causes its amplitude to decrease. The smaller the energy width is, the more localized the impurity state is, but the effect on scattering and optical properties can still be pronounced since the amplitude of the resonance at the same time is larger.

The behavior of the resonance position for the widest well ( $a=60$  Å) is slightly different from the other curves in Fig. 4. For this well width, the resonance is close to the subband bottom for central impurity positions. Therefore, the resonance profile becomes rather asymmetric, since it cannot be

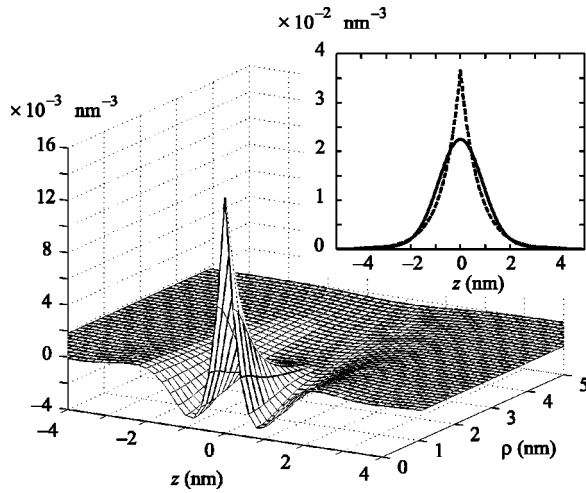


FIG. 6. The surface plot is the difference  $|\varphi_{1s}|^2 - |\psi_{QW}|^2$  for a wide (200 Å) Si/Si<sub>0.8</sub>Ge<sub>0.2</sub> quantum well, and the inset shows the QW envelope function  $|\psi_{QW}(z)|^2$  (solid) and the bulk variational function  $|\varphi_{1s}(z)|^2$  (dashed) for  $\rho=0$ . Both functions are normalized and give the Si bulk binding energy (29 meV; cf. Fig. 3).

continued below the lowest subband. The amplitude of the resonance, as measured by  $d_1(E_{\Sigma_u^*})$ , is furthermore very small as long as the resonance is close to the band bottom. At the same time the resonance width  $\Gamma$  is the largest for this well width, at intermediate impurity offsets. To accommodate this width, the resonance position shifts away from the subband bottom more quickly in this case than for the other well widths.

### C. The central-cell effect

The results discussed above for the ground-state binding energy indirectly contain the effect of strain, since this gives rise to the QW band offset, but do not include the central-cell effect, and therefore represent the effective-mass binding energy. To take the central cell into account for the two donor states attached to the lowest  $\Delta_{\perp}$  valleys is however straightforward by using Eq. (23). The bulk shifts  $\Delta_0$ ,  $\Delta_E$ , and  $\Delta_T$  depend on the particular impurity species (values for phosphorus are given in Sec. IV), and in addition we need to know the ratio of the QW and bulk envelope functions at the impurity position.

Regarding the bulk envelope function, one could imagine using a variational wave function, such as the normalized nonisotropic “hydrogenic” function

$$\varphi_{1s}(\rho, z) = \frac{1}{\sqrt{\pi a^2 b}} \exp\left(-\sqrt{\frac{\rho^2}{a^2} + \frac{z^2}{b^2}}\right) \quad (37)$$

originally used by Kohn and Luttinger<sup>42</sup> to obtain the value 29 meV for the effective-mass binding energy in Si (the energy is minimized by  $a=2.478$  nm and  $b=1.420$  nm). However, although variational functions may produce rather accurate estimates of the energy, they do not, in general, give a correct picture of the wave function. This is illustrated by Fig. 6, where we see that in the region close to the impurity,

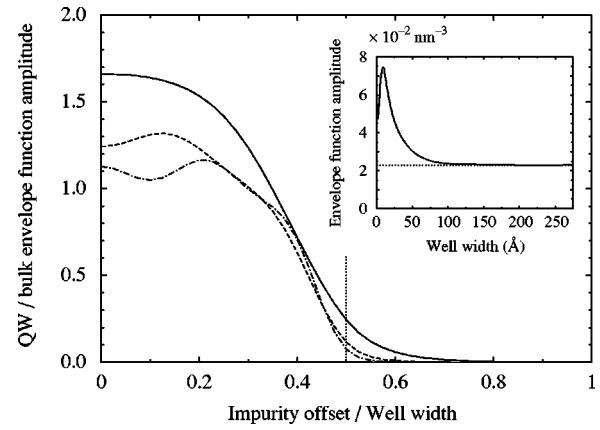


FIG. 7. The ratio of the QW envelope function amplitude to the bulk value, at the impurity position  $\mathbf{r}_0$ , for three different Si/Si<sub>0.8</sub>Ge<sub>0.2</sub> wells of widths (from top to bottom)  $a=30$  Å, 50 Å, and 70 Å. The vertical line marks the edge of the well, and the impurity offset is measured from the middle of the well. The bulk amplitude is defined as the wide-well limit ( $0.023 \text{ nm}^{-3}$ ) of the inset plot, which shows the QW envelope function amplitude as a function of the well width. The amplitude closely follows the variation of the ground-state binding energy (cf. Fig. 3), also for very narrow wells when both the binding energy and the amplitude again approach the bulk value.

the variational function  $\varphi_{1s}(\rho, z)$  given by Eq. (37) may differ substantially from the wave function  $\psi_{QW}(\rho, z)$  obtained with the basis expansion method, although they both reproduce the same binding energy. The two envelope functions do however agree very well in the exponentially decaying tail, which is precisely the part that determines the binding energy.

In the inset of Fig. 7, the value of the quantum well envelope function amplitude, at the impurity position, is plotted as a function of the well width. Comparing with Fig. 3 we see that at a width of 250 Å, the ground-state binding energy is extremely close to the variational value, which is reasonable since the well is much wider than the radius of the impurity state (estimated by  $a$  and  $b$ ). However, the QW envelope function amplitude differs substantially from  $|\varphi_{1s}(0,0)|^2 = 0.0365 \text{ nm}^{-3}$ . Instead, as the well becomes wider, the amplitude converges to a value of  $\approx 0.023 \text{ nm}^{-3}$ , which we therefore will take as the value for the bulk amplitude  $|\phi_{1s}(\mathbf{r}_0)|^2$ .

Once the bulk amplitude thus has been determined, we can use the ratio of the QW and bulk envelope functions, shown in Fig. 7, to evaluate the chemical shift for any well’s width and impurity position. When the impurity is close to the center of the well, the QW wave function in narrow wells is strongly enhanced at the impurity position, whereas for wider wells it approaches the bulk value. On the other hand, moving the impurity to the edge of the well leads to a rapid reduction of the ratio. It was mentioned in Sec. III that when we place the donor in the barrier, the wave function of the deep impurity states is localized in the well and not on the impurity. Now we find that even when the impurity is still inside the well, the wave-function maximum does not exactly coincide with the impurity position for asymmetric lo-

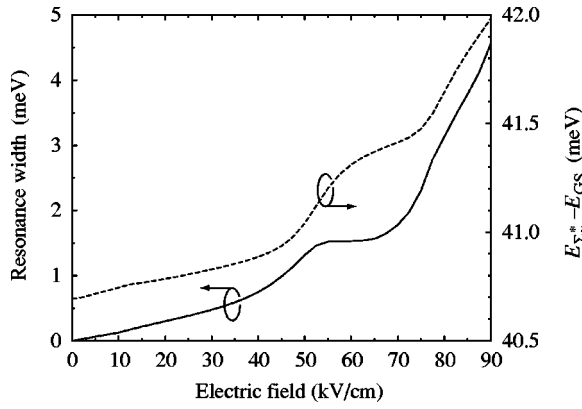


FIG. 8. The solid curve shows the energy width  $\Gamma$  of the resonant  $\Sigma_u^*$  state, as we apply a static transverse electric field to a Si/Si<sub>0.8</sub>Ge<sub>0.2</sub> well of width 55 Å. The impurities are placed in the center of the well. Also the energy separation (dashed curve) between the resonant state and the GS is presented.

cations. By studying the probability density one finds that the wave function is pushed towards the center of the well. One can view this as the wave function being reflected away by the barriers.

For wells wider than 50 Å, the ratio of the bulk and QW wave-function amplitudes is close to unity, and hence, as was mentioned in Sec. IV, the central-cell shift is substantially smaller in the quantum well than in bulk Si. For off-center impurity position this applies to even narrower wells (cf. Fig. 7). Note also that for very wide wells, the shift as calculated from Eq. (23) is different from that of bulk Si, due to the strain. Thus we can expect that the central-cell shifts are smaller in strained bulk Si than in the unstrained material. Since the chemical shift is much larger for impurities placed in the center of the well than for positions close to the barrier, the effective band of impurity energies mentioned above is furthermore widened by the central-cell effect.

#### D. Electric field and optical absorption

When a static electric field is applied across the quantum well, the parity symmetry is broken even when the impurities are placed in the center of the well, as in the case shown in Fig. 8. The energy width  $\Gamma$  of the resonant  $\Sigma_u^*$  state—and hence the degree of coupling—can be controlled by varying the electric field. Also the transition energy from the resonant state to the ground state can be fine-tuned in the same way, but the tuning range is small compared to the resonance width. By varying the QW parameters, on the other hand, this energy can be tuned over a vast range, as shown in the inset of Fig. 3.

As the electric field is increased from zero, the resonance width naturally also increases due to the induced coupling between the resonant state and the continuum. Still, the detailed behavior of the curves in Fig. 8 warrants further comments. If we take the energy of the zero-field conduction-band bottom as a fixed reference, we can study the field dependence of the energy positions of the impurity states and the quantum well levels (which are also shifted by the presence of the field). The positions of the second QW level and

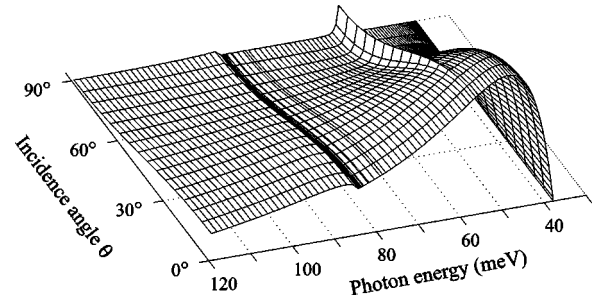


FIG. 9. The profile of the absorption cross section  $\sigma$  for a 40-Å wide Si/Si<sub>0.85</sub>Ge<sub>0.15</sub> quantum well, with the impurity offset 4 Å from the center of the well. The electron is initially assumed to be in the impurity ground state; the central-cell shift has however not been taken into account for the photon energy scale. For the actual values of the cross section, see Fig. 10. The coordinate system for the incidence angle  $\theta$  is defined in Sec. V.

the resonant  $\Sigma_u^*$  state—both of which have odd parity without any applied field—are practically unaffected by the field. On the other hand, the lowest QW level and the impurity ground state (even parity states) are deflected downwards. Hence, as the field is applied, the resonance appears at higher energies relative to the subband bottom. We noted above that the energy width is smaller for higher-energy resonances, and the interplay between this effect and the increase in the width from the stronger coupling gives rise to the plateau at about 50–70 kV/cm. At yet higher fields, the enhancement of the coupling will however dominate and the width increases again. Alternatively, one can consider that the electric field “pushes” the wave functions towards the side of the well. This affects odd and even states slightly differently, which influences the overlap between the first and second QW levels, and this is an essential factor in determining the coupling and the resonance position.

Finally we have also calculated the absorption cross section  $\sigma$  (cf. Figs. 9 and 10) from the donor ground state in the case when the  $\Sigma_u^*$  state is coupled to the first subband by placing the impurity asymmetrically in the well. According to the dipole selection rules, discussed in Sec. V, there is no absorption from the ground state to the unperturbed first sub-

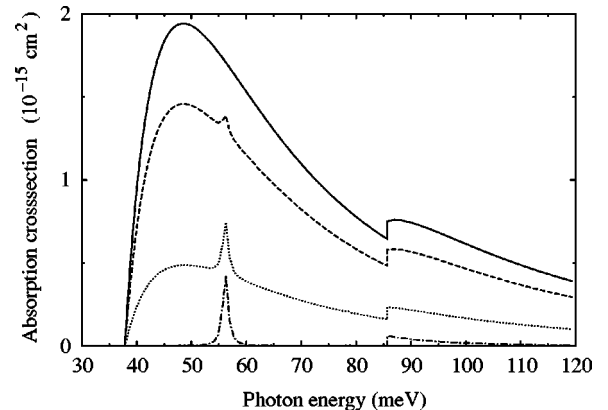


FIG. 10. For the same system as in Fig. 9 we here show the absorption cross section for some selected incidence angles  $\theta$ : from top to bottom  $\theta=0^\circ, 30^\circ, 60^\circ,$  and  $90^\circ$ .

band ( $q=0$ ) if the incoming light is linearly polarized along the QW growth direction. However, when the  $\Sigma_u^*$  state hybridizes with this subband, it mixes a certain amount of the second QW subband ( $q=1$ ) into the continuous states of the first subband, and thus  $\sigma_z \neq 0$ . Hence in an energy region, determined by the width  $\Gamma$ , around the resonant state, absorption is allowed even at normal incidence ( $\theta=90^\circ$ ). This is seen in the figures as the narrow peak at about 55 meV.

The shape of the normal incidence absorption peak is symmetric. This follows from the fact that due to the intra-subband selection rules, as shown in Sec. V, there is no interference between the matrix elements for absorption into the localized and continuous parts of the hybridized resonant state, respectively. Given this, and the energy-independent 2D density of states, the absorption spectrum will have the same shape as the resonance profile, which is symmetric in the displayed (and nearly all other) cases. Hence the asymmetry that often is observed in absorption spectra involving Fano resonances<sup>29,35–37</sup> is absent in our case.

For angles  $\theta < 90^\circ$ , absorption is also allowed for polarization parallel to the QW interfaces, given by  $\sigma_x$ , and this gives rise to the broad background peak. Furthermore, at about 85 meV photon energy, absorption into the second QW subband also becomes possible; in this case the selection rules allow absorption for any polarization. The cross section is finite at the second subband edge, reflecting the steplike 2D density of states.

The amplitude of the resonant-state absorption peak is not very large compared to the background, except for near-normal incidence ( $\theta \approx 90^\circ$ ). Nevertheless, the absorption cross section  $\sigma_z$  is still of the same order as the cross section for impurity absorption in bulk Si.<sup>56</sup> It is expected that the considered intrainpurity transition is particularly strong, since the transition is analogous to the so-called resonance line ( $2p \rightarrow 1s$ ) in atomic hydrogen.

## VII. SUMMARY AND DISCUSSION

In this paper we have presented a unified approach for calculating the energy levels of shallow donors in heterostructure quantum wells. By turning the Schrödinger equation—containing both the QW profile and the impurity potential—into a matrix eigenvalue problem, we obtain a complete description of the entire energy spectrum for all donor positions, both inside and outside the well.

Applying this method to Si/Si<sub>1-x</sub>Ge<sub>x</sub> quantum wells, we have calculated the binding energies of the ground state and the lowest antisymmetric resonant state for several well widths and impurity positions. The dependencies of the binding energies on the QW parameters follow the same general behavior found in variational calculations of GaAs/Al<sub>x</sub>Ga<sub>1-x</sub>As systems. When the donor is placed asymmetrically in the well, or a transverse electric field is applied, the resonant state can hybridize with the continuous subbands, and we can within our method evaluate the resonant-state energy width, which is directly related to the lifetime.

Si/Si<sub>1-x</sub>Ge<sub>x</sub> quantum wells are strained due to the lattice mismatch, and this was investigated in detail, along with the central-cell effect. By expressing the QW central-cell shift

through the parameters of the split donor states in bulk Si, and the amplitude ratio of the QW envelope function to the bulk one, it was shown that—depending on the impurity position and the well width—the QW shift can be either smaller or larger compared to the bulk case.

We have also compared the commonly used variational function for donors in bulk Si, to the ground-state wave function obtained with the basis expansion. Even though both functions give the same energy if the well is wide enough, they are far from identical. No assumption regarding the shape of the wave function is made in our nonvariational method, and we therefore conclude that the “hydrogenic” function is not capable of giving a correct description of the donor wave function. Instead we obtain the correct envelope functions of the localized, resonant and continuum eigenstates, and can then evaluate various matrix elements. As an example we present the ground-state optical-absorption spectrum, which shows a strong dependence on the direction of the incident photon compared to the quantum well axis due to the selection rules.

The possibility to populate the resonant state by electrically pumping the electrons in the QW subbands could be used to create a conduction-band resonant-state laser in a Si quantum well. Provided the carriers can reach the resonance energy without being scattered by other mechanisms, they can—through the hybridization—be captured into the localized part of the resonant state. They may then make an optical transition to the impurity ground state, a transition that is particularly strong, or to some excited localized state. Since, as was shown, the impurity states are attached to the QW levels, it is possible to tune the intrainpurity transition energies by varying the well parameters. The tuning range for the ground-state transition was shown to extend from 25 to 150 meV by changing the Si well width between 2 and 15 nm (the central-cell effect increases this range somewhat). Additionally, some fine-tuning could possibly be achieved by applying a transverse electric field.

For the Si wells we have considered, the resonance width can be as large as 10 meV, which gives a very short lifetime of about 0.1 ps. One may therefore expect that the resonant states can have a strong influence not only on the mobility, from the pronounced resonant scattering mechanism that appears in a narrow-energy region, but also on the noise spectrum, due to the capture and reemission process. These features are in fact present even when the impurities are placed outside the well, since there is coupling also between the shallow barrier donor state and the QW subbands.

## ACKNOWLEDGMENTS

This work was performed within the Nanometer Consortium at Lund University, and was supported by grants of the Swedish Foundation for Strategic Research, the Swedish Research Council (Grant No. TFR-THZ 2000-403), NorFA (Grant No. 000384), INTAS (Grant No. YSF 2002-95), the Russian Foundation for Basic Research, the Russian Academy of Science, and the Russian Ministry of Science. I.N.Y. is grateful for the support from the Wenner-Gren Foundation.

### APPENDIX A: RELATING THE CENTRAL-CELL PARAMETERS TO THE BINDING ENERGIES

In the effective-mass approximation, the wave function close to each conduction band minimum, i.e., in each valley  $\ell$ , is assumed to be of the form  $\psi_\ell(\mathbf{r}) = \phi(\mathbf{r})u_\ell(\mathbf{r})$ , with a common envelope function  $\phi$ . Here  $u_\ell$  is the Bloch function of the valley bottom, which can be written as  $u_\ell(\mathbf{r}) = \exp(i\mathbf{k}_\ell \cdot \mathbf{r})U_{\mathbf{k}_\ell}(\mathbf{r})$ , where  $\mathbf{k}_\ell$  is the wave vector of the respective conduction-band minimum, and  $U$  is a function with the periodicity of the lattice.

In bulk Si the six conduction-band minima  $\ell \in \{x, \bar{x}, y, \bar{y}, z, \bar{z}\}$  are degenerate. Therefore we write the wave function of each  $1s$  impurity state as

$$\Phi_{1s}^i(\mathbf{r}) = \phi_{1s}(\mathbf{r})u_i(\mathbf{r}) \quad (i = 1, \dots, 6), \quad (\text{A1})$$

with

$$u_i(\mathbf{r}) = \sum_{\ell} \alpha_{\ell}^i u_{\ell}(\mathbf{r}). \quad (\text{A2})$$

Using the valley bottom Bloch functions  $u_{\ell}$  as a basis, the Bloch functions  $u_i$  can thus be represented as vectors of the coefficients  $\alpha_{\ell}^i$ .

However, we also know that the six  $1s$  states transform as the  $T_d$  group, and hence their Bloch functions  $u_i$  can be written as<sup>43</sup>

$$\begin{aligned} u_A &= (1, 1, 1, 1, 1, 1)/\sqrt{6}, \\ u_E^{(1)} &= (1, 1, -1, -1, 0, 0)/2, \\ u_E^{(2)} &= (1, 1, 1, 1, -2, -2)/2\sqrt{3}, \\ u_T^{(1)} &= (1, -1, 0, 0, 0, 0)/\sqrt{2}, \\ u_T^{(2)} &= (0, 0, 1, -1, 0, 0)/\sqrt{2}, \\ u_T^{(3)} &= (0, 0, 0, 0, 1, -1)/\sqrt{2}. \end{aligned} \quad (\text{A3})$$

The label  $A$  refers to the nondegenerate ground state with energy  $-\Delta_0$  relative to the effective-mass value,  $E$  is the doublet state with energy  $-\Delta_0 + \Delta_E$ , and  $T$  is the triplet state with energy  $-\Delta_0 + \Delta_T$ .

Since the envelope function is assumed to vary slowly over distances comparable to the range of the central-cell potential  $V$ , we can write

$$\langle \Phi_{1s}^i | V | \Phi_{1s}^i \rangle = |\phi_{1s}(\mathbf{r}_0)|^2 \langle u_i | V | u_i \rangle, \quad (\text{A4})$$

where  $\mathbf{r}_0$  is the position of the impurity. The overlap matrix elements between Bloch functions from different valleys  $\ell$  are given in Eq. (21). By inserting the Bloch functions given in Eq. (A3) into Eq. (A4), we can express the donor energies in terms of  $V_0$ ,  $V_g$ , and  $V_f$  as follows:

$$\langle \Psi_A | V | \Psi_A \rangle = |\phi(\mathbf{r}_0)|^2 (V_0 + V_g + 4V_f) = -\Delta_0,$$

$$\langle \Psi_E | V | \Psi_E \rangle = |\phi(\mathbf{r}_0)|^2 (V_0 + V_g - 2V_f) = -\Delta_0 + \Delta_E,$$

$$\langle \Psi_T | V | \Psi_T \rangle = |\phi(\mathbf{r}_0)|^2 (V_0 - V_g) = -\Delta_0 + \Delta_T.$$

Inverting these relationships gives Eq. (22).

### APPENDIX B: DONOR STATES IN STRAINED SILICON

The strain Hamiltonian for the conduction band in Si can be written as<sup>57</sup>

$$\hat{H}_{\text{strain}} = \Xi_d \text{Tr}(\mathbf{e}) + \Xi_u (\hat{\mathbf{k}} \cdot \mathbf{e} \cdot \hat{\mathbf{k}}), \quad (\text{B1})$$

where  $\text{Tr}$  means the trace and  $\mathbf{e}$  is the strain tensor. The constants  $\Xi_d$  and  $\Xi_u$  are the deformation potentials, and  $\hat{\mathbf{k}}$  is a unit vector along one of the equivalent valleys  $\{x, \bar{x}, y, \bar{y}, z, \bar{z}\}$  in the unstrained material. In the basis of the valley bottom Bloch functions (cf. Appendix A),

$$\begin{aligned} \hat{H}_{\text{strain}} &= \frac{\Xi_u}{3} (e_{\parallel} - e_{\perp}) \begin{pmatrix} 1 & 0 & 0 & 0 & 0 & 0 \\ 0 & 1 & 0 & 0 & 0 & 0 \\ 0 & 0 & 1 & 0 & 0 & 0 \\ 0 & 0 & 0 & 1 & 0 & 0 \\ 0 & 0 & 0 & 0 & -2 & 0 \\ 0 & 0 & 0 & 0 & 0 & -2 \end{pmatrix} \\ &+ \left[ \Xi_d (2e_{\parallel} + e_{\perp}) + \frac{\Xi_u}{3} (2e_{\parallel} + e_{\perp}) \right] \mathbf{1}. \end{aligned} \quad (\text{B2})$$

The second term represents an overall shift and can be ignored altogether. Here  $\mathbf{1}$  is the  $6 \times 6$  unit matrix.

For a pseudomorphically (001)-grown strained layer, the strain tensor takes the form

$$\mathbf{e} = \begin{pmatrix} e_{\parallel} & 0 & 0 \\ 0 & e_{\parallel} & 0 \\ 0 & 0 & e_{\perp} \end{pmatrix}, \quad (\text{B3})$$

where  $e_{\parallel}$  and  $e_{\perp}$  are the strain tensor components parallel and perpendicular, respectively, to the interface planes. These can be expressed in terms of the unstrained lattice constants of the layer  $a_l$  and the substrate  $a_s$ , by evaluating the new lattice constants in the strained layer<sup>58</sup>

$$a_{\parallel} = a_s, \quad a_{\perp} = a_l \left[ 1 - \frac{2C_{12}}{C_{11}} \left( \frac{a_{\parallel}}{a_l} - 1 \right) \right], \quad (\text{B4})$$

where  $C_{ij}$  are the components of the stiffness tensor. We then have

$$e_{\parallel} = \frac{a_{\parallel}}{a_l} - 1, \quad e_{\perp} = \frac{a_{\perp}}{a_l} - 1 = -\frac{2C_{12}}{C_{11}} e_{\parallel}, \quad (\text{B5})$$

from which we see that the two components have opposite signs.

In order to take the effects of strain and the central cell into account simultaneously, we make a unitary transformation of  $\hat{H}_{\text{strain}}$  to the basis given by the states  $u_A$ ,  $u_E^{(i)}$ , and  $u_T^{(i)}$  defined in Appendix A, and add the central-cell contribution

$$\hat{H}_{cc} = -\Delta_0 \mathbf{1} + \begin{pmatrix} 0 & 0 & 0 & 0 & 0 & 0 \\ 0 & \Delta_E & 0 & 0 & 0 & 0 \\ 0 & 0 & \Delta_E & 0 & 0 & 0 \\ 0 & 0 & 0 & \Delta_T & 0 & 0 \\ 0 & 0 & 0 & 0 & \Delta_T & 0 \\ 0 & 0 & 0 & 0 & 0 & \Delta_T \end{pmatrix}, \quad (\text{B6})$$

which naturally is diagonal in this basis.

The resulting Hamiltonian matrix is, apart from a common diagonal constant  $-\Delta_0$ ,

$$\begin{pmatrix} 0 & 0 & -\sqrt{2}\xi & 0 & 0 & 0 \\ 0 & \Delta_E - \xi & 0 & 0 & 0 & 0 \\ -\sqrt{2}\xi & 0 & \Delta_E + \xi & 0 & 0 & 0 \\ 0 & 0 & 0 & \Delta_T - \xi & 0 & 0 \\ 0 & 0 & 0 & 0 & \Delta_T - \xi & 0 \\ 0 & 0 & 0 & 0 & 0 & \Delta_T + 2\xi \end{pmatrix}, \quad (\text{B7})$$

which is easily diagonalized; the once sixfold degenerate donor ground state splits into four nondegenerate and one twofold degenerate states (Ref. 43, Sec. 37), with energies

$$\epsilon_1 = -\Delta_0 + \Delta_E - \xi,$$

$$\epsilon_{2,3} = -\Delta_0 + \frac{\Delta_E}{2} (x + 1 \pm \sqrt{1 + 2x + 9x^2}), \quad (\text{B8})$$

$$\epsilon_{4,5} = -\Delta_0 + \Delta_T - \xi,$$

$$\epsilon_6 = -\Delta_0 + \Delta_T + 2\xi.$$

To abbreviate the expressions we have introduced

$$x = \xi / \Delta_E, \quad (\text{B9})$$

$$\xi = \Xi_u (e_{\perp} - e_{\parallel}) / 3 = -\frac{\Xi_u}{3} e_{\parallel} \left( \frac{2C_{12}}{C_{11}} + 1 \right). \quad (\text{B10})$$

The Bloch functions of the six eigenstates are<sup>59</sup>

$$\begin{aligned} u_1 &= (1, 1, -1, -1, 0, 0) / 2, \\ u_2 &= (\alpha u_A + u_E^{(2)}) / \sqrt{1 + \alpha^2}, \\ u_3 &= (u_A - \alpha u_E^{(2)}) / \sqrt{1 + \alpha^2}, \\ u_4 &= (1, -1, 0, 0, 0, 0) / \sqrt{2}, \\ u_5 &= (0, 0, 1, -1, 0, 0) / \sqrt{2}, \\ u_6 &= (0, 0, 0, 0, 1, -1) / \sqrt{2}, \end{aligned} \quad (\text{B11})$$

expressed in the valley bottom Bloch function basis (cf. Appendix A) with  $u_A$  and  $u_E^{(2)}$  given in Eq. (A3), and

$$\alpha = \frac{-2x\sqrt{2}}{1 + x + \sqrt{1 + 2x + 9x^2}}. \quad (\text{B12})$$

If the strain splitting  $\Xi_u (e_{\perp} - e_{\parallel})$  is much larger than the central-cell splitting  $\Delta_E$ , as is the typical situation in Si grown on a  $\text{Si}_{1-x}\text{Ge}_x$  substrate,<sup>53</sup>  $x \gg 1$  and  $\alpha \approx -1/\sqrt{2}$ . In this limit the eigenfunctions  $u_2$  and  $u_3$  become

$$\begin{aligned} u_2 &\approx (0, 0, 0, 0, 1, 1) / \sqrt{2}, \\ u_3 &\approx (1, 1, 1, 1, 0, 0) / 2, \end{aligned} \quad (\text{B13})$$

with energies

$$\begin{aligned} \epsilon_2 &\approx 2\xi - \Delta_0 + \frac{2\Delta_E}{3}, \\ \epsilon_3 &\approx -\xi - \Delta_0 + \frac{\Delta_E}{3}. \end{aligned} \quad (\text{B14})$$

Thus in this case the six states separate into two groups, where  $u_2$  and  $u_6$  are comprised of the two  $k_z$  valleys, and the four other states are not coupled to these valleys at all.

In the opposite limit, if the strain is very small,  $x \ll 1$  and we see that  $u_1$  and  $u_2$  originate from the doublet and  $u_3$  from the ground state.

<sup>1</sup>A. Blom, M.A. Odnoblyudov, H.H. Cheng, I.N. Yassievich, and K.A. Chao, *Appl. Phys. Lett.* **79**, 713 (2001).

<sup>2</sup>I.V. Altukhov, E.G. Chirkova, V.P. Sinis, M.S. Kagan, Y.P. Gousev, S.G. Thomas, K.L. Wang, M.A. Odnoblyudov, and I.N. Yassievich, *Appl. Phys. Lett.* **79**, 3909 (2001).

<sup>3</sup>S.A. Lynch *et al.*, *Mater. Sci. Eng.*, B **89**, 10 (2002).

<sup>4</sup>G. Masini, L. Colace, and G. Assanto, *Mater. Sci. Eng.*, B **89**, 2 (2002).

<sup>5</sup>D.D. Arnone, C.M. Ciesla, and M. Pepper, *Phys. World* **13** (4), 35 (2000).

<sup>6</sup>G. Bastard, *Phys. Rev. B* **24**, 4714 (1981).

<sup>7</sup>R.L. Greene and K.K. Bajaj, *Solid State Commun.* **45**, 825

(1983).

<sup>8</sup>R.L. Greene and K.K. Bajaj, *Phys. Rev. B* **31**, 4006 (1985).

<sup>9</sup>S. Fraizzoli, F. Bassani, and R. Buczko, *Phys. Rev. B* **41**, 5096 (1990).

<sup>10</sup>F.J. Betancur and I.D. Mikhailov, *Phys. Rev. B* **51**, 4982 (1995).

<sup>11</sup>K. Jayakumar, S. Balasubramanian, and M. Tomak, *Phys. Rev. B* **34**, 8794 (1986).

<sup>12</sup>W.T. Masselink, Y.-C. Chang, and H. Morkoç, *Phys. Rev. B* **32**, 5190 (1985).

<sup>13</sup>A. Pasquarello, L.C. Andreani, and R. Buczko, *Phys. Rev. B* **40**, 5602 (1989).

<sup>14</sup>M. Stopa and S. DasSarma, *Phys. Rev. B* **40**, 8466 (1989).

- <sup>15</sup>J.P. Loehr and J. Singh, Phys. Rev. B **41**, 3695 (1990).
- <sup>16</sup>V.Y. Aleshkin, B.A. Andreev, V.I. Gavrilenko, I.V. Erofeeva, D.V. Kozlov, and O.A. Kuznetsov, Fiz. Tekh. Poluprovodn. **34**, 582 (2000) [Semiconductors **34**, 563 (2000)].
- <sup>17</sup>R.C. Miller, A.C. Gossard, W.T. Tsang, and O. Munteanu, Phys. Rev. B **25**, 3871 (1982).
- <sup>18</sup>B. Lambert, B. Deveauda, A. Regrenya, and G. Talalaeffa, Solid State Commun. **43**, 443 (1982).
- <sup>19</sup>B.V. Shanabrook and J. Comas, Surf. Sci. **142**, 504 (1984).
- <sup>20</sup>B.V. Shanabrook, J. Comas, T.A. Perry, and R. Merlin, Phys. Rev. B **29**, 7096 (1984).
- <sup>21</sup>N.C. Jarosik, B.D. McCombe, B.V. Shanabrook, J. Comas, J. Ralston, and G. Wicks, Phys. Rev. Lett. **54**, 1283 (1985).
- <sup>22</sup>J.A. Brum, G. Bastard, and C. Guillemot, Phys. Rev. B **30**, 905 (1984).
- <sup>23</sup>S. Pantelides and C.T. Sah, Solid State Commun. **11**, 1713 (1972).
- <sup>24</sup>R. Buczko and F. Bassani, Phys. Rev. B **45**, 5838 (1992).
- <sup>25</sup>N. Binggeli and A. Baldereschi, Phys. Rev. B **45**, 5944 (1992).
- <sup>26</sup>N.O. Lipari, A. Baldereschi, and M.L.W. Thewalt, Solid State Commun. **33**, 277 (1980).
- <sup>27</sup>E.R. Mueller, D.M. Larsen, J. Waldman, and W.D. Goodhue, Phys. Rev. B **49**, 13475 (1994).
- <sup>28</sup>H.P. Wagner and W. Prettl, Solid State Commun. **66**, 367 (1988).
- <sup>29</sup>U. Fano, Phys. Rev. **124**, 1866 (1961).
- <sup>30</sup>A. Onton, P. Fisher, and A.K. Ramdas, Phys. Rev. **163**, 686 (1967).
- <sup>31</sup>A. Onton, Phys. Rev. B **4**, 4449 (1971).
- <sup>32</sup>E. Goldys, P. Galtier, G. Martinez, and I. Gorczyca, Phys. Rev. B **36**, 9662 (1987).
- <sup>33</sup>M.A. Odnoblyudov, I.N. Yassievich, V.M. Chistyakov, and K.A. Chao, Phys. Rev. B **62**, 2486 (2000).
- <sup>34</sup>F. Capasso, C. Sirtori, J. Faist, D.L. Sivco, S.-N.G. Chu, and A.Y. Cho, Nature (London) **358**, 565 (1992).
- <sup>35</sup>C. Sirtori, F. Capasso, J. Faist, and S. Scandolo, Phys. Rev. B **50**, 8663 (1994).
- <sup>36</sup>D.Y. Oberli, G. Böhm, G. Weimann, and J.A. Brum, Phys. Rev. B **49**, 5757 (1994).
- <sup>37</sup>S. Glutsch, D.S. Chemla, and F. Bechstedt, Phys. Rev. B **51**, 16 885 (1995).
- <sup>38</sup>A. Blom, M.A. Odnoblyudov, I.N. Yassievich, and K.A. Chao, Phys. Rev. B **65**, 155302 (2002).
- <sup>39</sup>C. Priester, G. Allan, and M. Lannoo, Phys. Rev. B **29**, 3408 (1984).
- <sup>40</sup>S.T. Yen, Phys. Rev. B **66**, 075340 (2002).
- <sup>41</sup>A. Blom, M.A. Odnoblyudov, I.N. Yassievich, and K.A. Chao, Phys. Status Solidi B **235**, 85 (2003).
- <sup>42</sup>W. Kohn and J.M. Luttinger, Phys. Rev. **98**, 915 (1955).
- <sup>43</sup>G.L. Bir and G.E. Pikus, *Symmetry and Strain-Induced Effects in Semiconductors* (Wiley, New York, 1974).
- <sup>44</sup>A.A. Prokof'ev, M.A. Odnoblyudov, and I.N. Yassievich, Fiz. Tekh. Poluprovodn. **35**, 586 (2001) [Semiconductors **35**, 565 (2001)].
- <sup>45</sup>A.A. Prokof'ev, I.N. Yassievich, A. Blom, M.A. Odnoblyudov, and K.A. Chao, Nanotechnology **12**, 457 (2001).
- <sup>46</sup>T.A. Perry, R. Merlin, B.V. Shanabrook, and J. Comas, Phys. Rev. Lett. **54**, 2623 (1985).
- <sup>47</sup>M. Helm, F.M. Peeters, F. DeRosa, E. Colas, J.P. Harbison, and L.T. Florez, Phys. Rev. B **43**, 13 983 (1991).
- <sup>48</sup>G. Bastard, J.A. Brum, and R. Ferreira, in *Solid State Physics*, edited by H. Ehrenreich and D. Turnbull (Academic Press, San Diego, 1991), Vol. 44, p. 229.
- <sup>49</sup>J.H. Davies, *The Physics of Low-Dimensional Semiconductors* (Cambridge University Press, Cambridge, 1998).
- <sup>50</sup>R.A. Faulkner, Phys. Rev. **184**, 713 (1969).
- <sup>51</sup>C. Jagannath, Z.W. Grabowski, and A.K. Ramdas, Phys. Rev. B **23**, 2082 (1981).
- <sup>52</sup>S.V. Gastev, E.Z. Imamov, N.S. Sokolov, and I.N. Yassievich, Zh. Éksp. Teor. Fiz. **90**, 1830 (1986) [Sov. Phys. JETP **63**, 1073 (1986)].
- <sup>53</sup>M.M. Rieger and P. Vogl, Phys. Rev. B **48**, 14 276 (1993).
- <sup>54</sup>J.P. Dismukes, L. Ekstrom, and R.J. Paff, J. Phys. Chem. **68**, 3021 (1964).
- <sup>55</sup>H. Yaguchi, K. Tai, K. Takemasa, K. Onabe, R. Ito, and Y. Shiraki, Phys. Rev. B **49**, 7394 (1994).
- <sup>56</sup>R. Baron, M.H. Young, J.K. Neeland, and O.J. Marsh, Appl. Phys. Lett. **30**, 594 (1977).
- <sup>57</sup>C. Herring and E. Vogt, Phys. Rev. **101**, 944 (1956).
- <sup>58</sup>C.G. Van de Walle, Phys. Rev. B **39**, 1871 (1989).
- <sup>59</sup>The states  $u_2$  and  $u_3$  differ slightly from those given in Eq. (37.14) of Ref. 43; the states given there are not, as claimed, eigenstates of the Hamiltonian (B7).